Quantum and temperature effects on Davydov soliton dynamics. IV. Lattice with a thermal phonon distribution

1993 J. Phys.: Condens. Matter 5 3883

(http://iopscience.iop.org/0953-8984/5/23/015)

J. Phys.: Condens. Matter 5 (1993) 3883–3896. Printed in the UK

Quantum and temperature effects on Davydov soliton dynamics: IV. Lattice with a thermal phonon distribution

Wolfgang Förner

Chair for Theoretical Chemistry and Laboratory of the National Foundation of Cancer Research, Friedrich-Alexander University Erlangen–Nürnberg, Egerlandstrasse 3, W-8520 Erlangen, Federal Republic of Germany

Received 21 December 1992

Abstract. We derive equations of motion for a new model to introduce temperature effects into Davydov's $|D_1\rangle$ theory for solitons in proteins. The temperature model used so far suffers from conceptual difficulties, although it can reproduce exact quantum Monte Carlo (QMC) results qualitatively correctly as was shown in part II of this series. In our model we populate the lattice with a thermal phonon distribution and derive equations of motion in the presence of these thermal phonons, instead of deriving equations of motion from a thermally averaged Hamiltonian as in Davydov's theory. This procedure seems to be more reliable than Davydov's averaged Hamiltonian approach. For derivation of the equations of motion the Euler–Lagrange method is used. Numerical applications to soliton dynamics at 300 K are reported and comparisons of the results obtained with available exact QMC data are discussed. It is found that Davydov's method agrees better with the QMC results than does the newly derived method, although the latter method seems to be physically more reliable.

1. Introduction

For the mechanism of energy transport through proteins, Davydov and Kislukha [1] and Davydov [2] suggested that the energy of about 0.4 eV released by hydrolysis of adenosine-triphosphate could be transported in quanta of the amide-I (mainly C–O stretch) vibration (about 0.2 eV). The CO groups participate in hydrogen bonds which form chains parallel to the axis of α-helical proteins. Thus the amide-I vibration interacts with the acoustic phonons in these chains. The region in which the vibrational energy is localized can travel as a soliton along the chain [1, 2]. In the original theory [1], an *ansatz* was used for the wavefunction ($|D_2\rangle$) which treats the lattice classically. At zero temperature it has been confirmed that Davydov solitons exist for parameter values appropriate for proteins [3]. Also their stability against disorder along the chain was studied [4]. The investigation of temperature lead to controversial results. For a short review see part II of this series [5] and for details see, e.g., [6–13]. Also there and in [14–22], shortcomings of the different *ansatz* states and of the derivation of equations of motion from them are discussed.

We also used the Langrangian method described in [17] to obtain correct equations of motion for the $|D_1\rangle$ *ansatz* state from the thermally averaged Hamiltonian derived in [2, 15]. In this investigation [19, 20] (part I of this series is [20]), as well as in our previous studies within the $|D_2\rangle$ state, summarized in [19] we found that Davydov solitons should be stable at 300 K if the spring constant of the hydrogen bonds is larger than previously assumed. Since all our results indicate that the hydrogen bond spring constant should be large to allow soliton formation at 300 K, we reconsidered the suggestion of Scott [3, 5, 24] that

0953-8984/93/233883+14$07.50

in one-chain simulations the spring constant should be larger by a factor of 3, in order to simulate the three coupled chains present in real protein α-helices within a one-chain model. For an excellent review of the state of art of work on Davydov solitons the reader should consult Scott's recent paper [23]. We could confirm Scott's conclusion (in the case of the $|D_2\rangle$ *ansatz*) about parameter values also for excitations that he did not consider, and for which his analytical considerations do not hold. However, within the $|D_1\rangle$ model we found that for the symmetric A mode the equations of motion for one spine and for three coupled chains are identical [24] (part III of this series). In simulations on three coupled chains we found that also in this case the soliton stability at 300 K requires a hydrogen bond spring constant larger than roughly 30 N m^{-1}. However, since the value of 13 N m^{-1} is taken from crystalline formamide where only hydrogen-bonded molecules vibrate, while in proteins covalently bound peptide units are moving, we consider 30–40 N m^{-1} for this constant as not unrealistic.

There are doubts whether the Davydov concept of using a thermally averaged Hamiltonian to derive equations of motion from it is in agreement with statistical mechanics. There is the possibility that it may provide results which are even qualitatively misleading. Therefore we performed [5] a comparison of our results obtained with the averaged Hamiltonian method with the exact quantum Monte Carlo (QMC) results of Wang *et al* [21]. We found that the *ansatz* of Davydov is quantitatively incorrect; however, it describes the qualitative features reported in [21] correctly. The $|D_2\rangle$ state models and the partial dressing theory of Brown and Ivic [25] fail to reproduce the results of [21] even qualitatively. Owing to the conceptual difficulties with Davydov's temperature model and its failure to reproduce quantitative QMC results at least approximately we present in this work a new model for incorporation of temperature effects into $|D_1\rangle$ theory. Numerical applications of the new model as well as comparisons of the results with the QMC data are discussed.

2. Method

The Hamiltonian on which Davydov's soliton concept is based is [1]

$$\hat{H} = \sum_n \left[E_0 \hat{a}_n^+ \hat{a}_n - J(\hat{a}_n^+ \hat{a}_{n+1} + \hat{a}_{n+1}^+ \hat{a}_n) + \frac{\hat{p}_n^2}{2M} + \frac{W}{2}(\hat{q}_{n+1} - \hat{q}_n)^2 + X \hat{a}_n^+ \hat{a}_n (\hat{q}_{n+1} - \hat{q}_n) \right]. \tag{1}$$

In equation (1), $\hat{a}_n^+$ and $\hat{a}_n$ are the usual boson creation and annihilation operators [3], respectively, for the amide-I oscillators at sites n (figure 1). From infrared spectra the ground-state energy of an isolated amide-I oscillator can be deduced ($E_0 = 0.205$ eV). Usually for all parameters in equation (1) the site-independent mean values are used. The average value for the dipole–dipole coupling between neighbouring amide-I oscillators is $J = 0.967$ meV. The average spring constant of the hydrogen bonds is usually taken to be $W = 13$ N m^{-1}, $\hat{p}_n$ is the momentum and $\hat{q}_n$ the position operator of unit n. The average mass M is taken to be that of myosine ($M = 114 m_p$; m_p is the proton mass). The energy of the CO stretching vibration in hydrogen bonds is a function of the length r of the hydrogen bond ($E = E_0 + Xr$). For X the experimental estimates are 35 pN and 62 pN. *Ab-initio* calculations on formamide dimers usually lead to $X = 30$–50 pN; however, with small-basis-set *ab-initio* calculations, even negative values for X were obtained (see, e.g., [23] for a review and references).

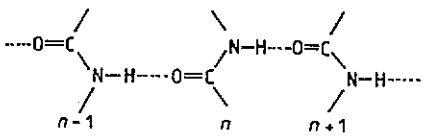

Figure 1. Schematic picture of a hydrogen-bonded channel in a protein.

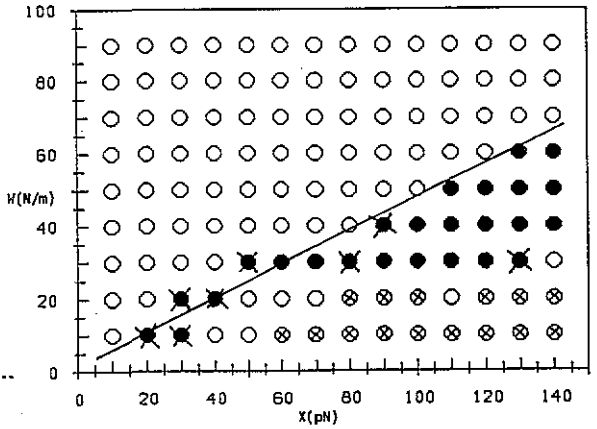

Figure 2. Survey of the (X, W) parameter space for an initial excitation at site 24 in a chain of 25 units at 300 K using a model with a thermal phonon population of the lattice: ○, dispersive system; ●, travelling soliton; ●, crossed, slowly dispersing travelling solitary wave; ⊗, trapped excitation.

The Hamiltonian [1, 2] in a second quantized form including disorder is given by

$$\hat{H} = \sum_n [(E_0 + E_n)\hat{a}_n^+\hat{a}_n - J_n(\hat{a}_{n+1}^+\hat{a}_n + \hat{a}_n^+\hat{a}_{n+1})]$$

$$+ \sum_k \hbar\omega_k \left[\hat{b}_n^+\hat{b}_k + \tfrac{1}{2} + \sum_n B_{nk}(\hat{b}_k + \hat{b}_k^+)\hat{a}_n^+\hat{a}_n\right]$$

$$B_{nk} = (X_n/\omega_k)(1/\sqrt{2\hbar\omega_k})[U_{n+1,k}/\sqrt{M_{n+1}} - U_{nk}/\sqrt{M_n}]. \tag{2}$$

$\hat{b}_k^+$ and $\hat{b}_k$ are creation and annihilation operators, respectively, for acoustic phonons of wavenumber k. The translational mode has to be excluded from the summation. Note that in the simulations reported in section 3 we again use the asymmetric interaction model where only the coupling of the oscillator n to the hydrogen bond between n and $n+1$ in which the oscillator takes part is considered. For our comparison with QMC data [21] in section 4, however, we had to introduce also the symmetric interaction as well as cyclic boundary conditions [5] since the only available exact QMC results [21] were obtained for this case. ω_k denotes the eigenfrequency of the normal mode k and **U** contains the normal mode coefficients. ω and **U** are obtained by numerical diagonalization of the matrix **V** with elements

$$V_{nm} = \{[W_n(1-\delta_{nN}) + W_{n-1}(1-\delta_{n1})]\delta_{nm} - W_n(1-\delta_{nN})\delta_{m,n+1}$$
$$- W_{n-1}(1-\delta_{n1})\delta_{m,n-1}\}(M_n M_m)^{-1/2}. \tag{3}$$

The form of **V** implies that we use free chain ends and N units. Other boundary conditions such as cyclic [15], as used in section 4 (see [5] for details) or fixed chain ends [16] require another form of **V** [5].

In our modified *ansatz* we use a lattice already prepared with a thermal phonon distribution $|T\rangle$ as we did in case of the classical $|D_2\rangle$ *ansatz* state [12] instead of starting

from a thermally averaged Lagrangian:

$$|D_1, T\rangle = \sum_n a_n(t)\hat{a}_n^+|0\rangle_e \hat{W}_n|T\rangle. \tag{4}$$

Here $|0\rangle_e$ is the exciton vacuum, $|a_n(t)|^2$ are the probabilities of finding an amide-I vibrational quantum at site n, and $\hat{W}_n$ is a unitary displacement operator:

$$\hat{W}_n = \exp(\hat{S}_n) \qquad \hat{S}_n = \sum_k [b_{nk}(t)\hat{b}_k^+ - b_{nk}^*(t)\hat{b}_k]. \tag{5}$$

Here $|b_{nk}(t)|^2$ is the number of phonons excited by exciton–phonon coupling in the lattice at site n and wavenumber k, and $|T\rangle$ is a coherent state with $|B_k|^2$ thermal phonons in each normal mode k:

$$|T\rangle = \exp(\hat{T})|0\rangle_p \qquad \hat{T} = \sum_k (B_k\hat{b}_k^+ - B_k^*\hat{b}_k). \tag{6}$$

$|B_k|^2$ is computed according to Bose–Einstein statistics:

$$|B_k|^2 = 1/[\exp(\hbar\omega_k/k_BT) - 1] \equiv v_k^2. \tag{7}$$

$|T_k\rangle$ is an exact solution of the time-dependent Schrödinger equation

$$i\hbar(\partial/\partial t)|T_k\rangle = \hbar\omega_k(\hat{b}_k^+\hat{b}_k + \tfrac{1}{2})|T_k\rangle \tag{8}$$

if

$$B_k(t) = |B_k|\exp(-i\omega_k t). \tag{9}$$

Further

$$\hat{U}_{nk}|T_k\rangle = \exp(\hat{S}_{nk})\exp(\hat{T}_k)\,|0\rangle_p = \exp(\tfrac{1}{2}[\hat{S}_{nk}, \hat{T}_k])\exp(\hat{S}_{nk} + \hat{T}_k)\,|0\rangle_p. \tag{10}$$

Here $|0\rangle_p$ denotes the phonon vacuum. With

$$[\hat{S}_{nk}, \hat{T}_k] = b_{nk}B_k^* - b_{nk}^*B_k \tag{11}$$

we obtain our final *ansatz* state as

$$|\Psi\rangle = |D_1, T\rangle = \sum_n a_n(t)\hat{a}_n^+|0\rangle_e \exp\left(\tfrac{1}{2}\sum_k (b_{nk}B_k^* - b_{nk}^*B_k)\right)$$
$$\times \exp\left(\sum_k (c_{nk}\hat{b}_k^+ - c_{nk}^*\hat{b}_k)\right)|0\rangle_p \tag{12}$$

where

$$c_{nk}(t) = b_{nk}(t) + V_k\exp(-i\omega_k t). \tag{13}$$

Thus the phonon part consists of coherent states with amplitudes $c_{nk}(t)$, modulated by a phase factor. Then the Lagrangian is given by (see [17] for details of the method)

$$L = \tfrac{1}{2}i\hbar(\langle\Psi|\partial\Psi/\partial t\rangle - \langle\partial\Psi/\partial t|\Psi\rangle) - H = L_t - H + \tfrac{1}{2}i\hbar\sum_{nk}|a_n|^2 v_k[(\dot{b}_{nk} + i\omega_k b_{nk}) \times \exp(i\omega_k t) - (\dot{b}^*_{nk} - i\omega_k b^*_{nk})\exp(-i\omega_k t)]. \tag{14}$$

Thus

$$L_t = \tfrac{1}{2}i\hbar\left\{\sum_n(\dot{a}_n a^*_n - \dot{a}^*_n a_n) + \sum_{nk}|a_n|^2(\dot{c}_{nk}c^*_{nk} - \dot{c}^*_{nk}c_{nk})\right\} \tag{15}$$

$$L = \tfrac{1}{2}i\hbar\sum_n\Big[\!\Big[(\dot{a}_n a^*_n - \dot{a}^*_n a_n) + \sum_k|a_n|^2\{(\dot{b}_{nk}b^*_{nk} - \dot{b}^*_{nk}b_{nk}) - 2i\omega_k v_k^2 + 2v_k[\dot{b}_{nk}\exp(i\omega_k t) - \dot{b}^*_{nk}\exp(-i\omega_k t)]\}\Big]\!\Big] - H \tag{16}$$

and

$$H = \langle D_1, T|\hat{H}|D_1, T\rangle = \sum_n\Big[\!\Big[(E_0 + E_n)|a_n|^2 - J_n a^*_n a_{n+1}D_{n,n+1} - J_{n-1}a^*_n a_{n-1}D_{n,n-1} + |a_n|^2\sum_k\hbar\omega_k\{B_{nk}[b_{nk} + b^*_{nk} + 2v_k\cos(\omega_k t)] + |b_{nk}|^2 + v_k^2 + \tfrac{1}{2} + v_k[b_{nk}\exp(i\omega_k t) + b^*_{nk}\exp(-i\omega_k t)]\}\Big]\!\Big] \tag{17}$$

$$D_{nm} = \exp\left(\sum_k[b^*_{nk}b_{mk} - \tfrac{1}{2}(|b_{nk}|^2 + |b_{mk}|^2) + (b^*_{nk} - b^*_{mk})v_k\exp(-i\omega_k t) - (b_{nk} - b_{mk})v_k\exp(i\omega_k t)]\right). \tag{18}$$

Note, that in contrast with Davydov's model, the exponent in D_{nm} contains no temperature-dependent real part (besides the implicit temperature dependence in the b_{nk}) and thus there is nothing like a Debye–Waller factor present. From this, equations of motion are obtained with the help of the Euler–Lagrange equations:

$$(d/dt)(\partial L/\partial\dot{a}^*_n) - \partial L/\partial a^*_n = 0 \qquad (d/dt)(\partial L/\partial\dot{b}^*_{nk}) - \partial L/\partial b^*_{nk} = 0. \tag{19}$$

In [17] it is shown that for the $|D_1\rangle$ state the Euler–Lagrange method leads to the same equations of motion as projection techniques, time-dependent variational principle and Heisenberg operator equations, while Davydov's method [15] (treating $\langle D_1|\hat{H}|D_1\rangle$ as a classical Hamiltonian function) leads to different equations of motion, which do not even reproduce special analytically soluble cases ($J = 0$).

From the Euler–Lagrange equations we obtain

$$i\hbar\dot{a}_n + \tfrac{1}{2}i\hbar a_n\sum_k\{(\dot{b}_{nk}b^*_{nk} - \dot{b}^*_{nk}b_{nk}) - 2i\omega_k v_k^2 + 2v_k[\dot{b}_{nk}\exp(i\omega_k t) - \dot{b}_{nk}\exp(-i\omega_k t)]\} = \frac{\partial H}{\partial a^*_n}. \tag{20}$$

After differentiation of H and performing the phase transformation $a_n(t) = a'_n(t)\exp(-iE_0t/\hbar)$ we obtain the equation of motion (note that we have changed a'_n to a_n after the transformation again):

$$\begin{aligned} i\hbar\dot{a}_n = &-(J_n a_{n+1} D_{n,n+1} + J_{n-1} a_{n-1} D_{n,n-1}) + E_n a_n \\ &- \tfrac{1}{2} i\hbar a_n \sum_k [(\dot{b}_{nk} b^*_{nk} - \dot{b}^*_{nk} b_{nk}) + 2v_k[\dot{b}_{nk}\exp(i\omega_k t) - \dot{b}^*_{nk}\exp(-i\omega_k t)]] \\ &+ a_n \sum_k \hbar\omega_k \{B_{nk}[b_{nk} + b^*_{nk} + 2v_k\cos(\omega_k t)] + |b_{nk}|^2 \\ &+ v_k[b_{nk}\exp(i\omega_k t) + b^*_{nk}\exp(-i\omega_k t)]\}. \end{aligned} \tag{21}$$

From this equation we obtain the expression

$$i\hbar(\dot{a}^*_n a_n + \dot{a}_n a^*_n) = -J_n(a^*_n a_{n+1} D_{n,n+1} - a_n a^*_{n+1} D_{n+1,n}) - J_{n-1}(a^*_n a_{n-1} D_{n,n-1} - a_n a^*_{n-1} D_{n-1,n}) \tag{22}$$

which summed over n leads to the conservation of the norm of our wavefunction. From the second Euler–Lagrange equation we obtain

$$i\hbar|a_n|^2\dot{b}_{nk} + \tfrac{1}{2}i\hbar[b_{nk} + 2v_k\exp(-i\omega_k t)](\dot{a}^*_n a_n + \dot{a}_n a^*_n) = (\partial H/\partial b^*_{nk}) - \hbar\omega_k|a_n|^2 v_k\exp(-i\omega_k t). \tag{23}$$

Substitution of the above result for the time derivative of the absolute square of a_n and differentiation of H with respect to b^*_{nk} lead to the equations of motion

$$i\hbar\dot{b}_{nk} = \hbar\omega_k(B_{nk} + b_{nk}) - J_n D_{n,n+1}(b_{n+1,k} - b_{nk})a_{n+1}/a_n - J_{n-1} D_{n,n-1}(b_{n-1,k} - b_{nk})a_{n-1}/a_n. \tag{24}$$

This equation is the same as that for the $|D_1\rangle$ state without inclusion of temperature effects because the thermal motions of the lattice and those which originate from the coupling to the oscillators are separated. Temperature enters only implicitly via the a-, b- and D-values. This is the same situation as in the case of the $|D_2\rangle$ state with a thermally populated lattice [12, 13, 19]. As in that case, also in equation (21) we could formally perform an integration over time and the phase transformation

$$\begin{aligned} a_n(t) = a'_n(t)\exp\Bigg(&-2i\sum_k v_k \int_0^t \{\mathrm{Im}[\dot{b}_{nk}(t')\exp(i\omega_k t')] \\ &+ \omega_k\cos(\omega_k t') + \omega_k\,\mathrm{Re}[b_{nk}(t')\exp(i\omega_k t')]\}\,dt'\Bigg). \end{aligned} \tag{25}$$

Then as in case of the $|D_2\rangle$ state the effects of the thermally populated lattice appear explicitly only as site- and time-dependent phase factors at the J_n-values in the equations of motion. Because of the denominators a_n in equation (24) we have again to start the time simulation with an initial excitation of the form described in [20]. Note that this approach does not start from a thermally averaged Hamiltonian as Davydov's method does, but from an initial state with a lattice prepared with a thermal distribution of phonons.

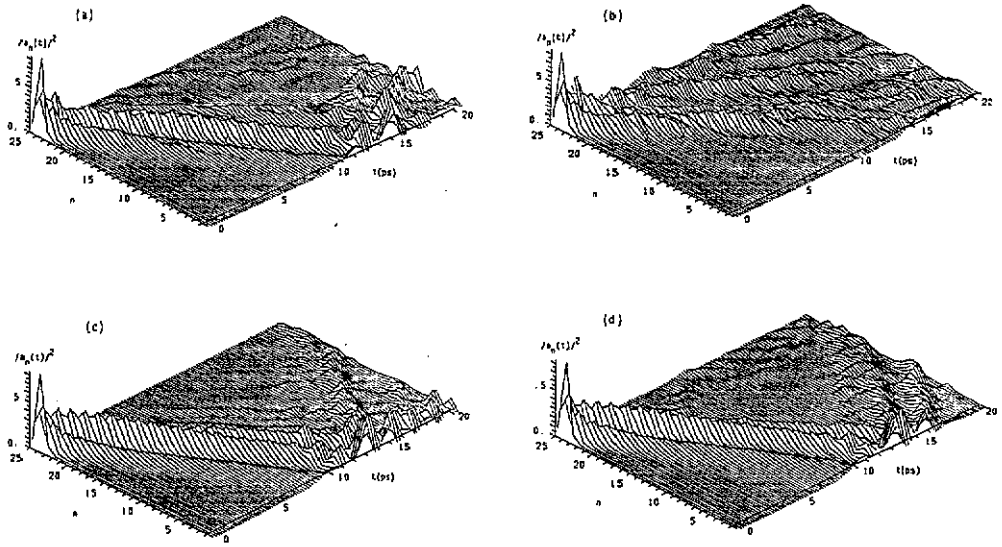

Figure 3. The probability of finding a quantum of amide-I vibration $|a_n(t)|^2$ as a function of site n and time t at 300 K for different parameter values: (*a*) $W = 15$ N m^{-1}, $X = 40$ pN; (*b*) $W = 15$ N m^{-1}, $X = 60$ pN; (*c*) $W = 30$ N m^{-1}, $X = 50$ pN; (*d*) $W = 30$ N m^{-1}, $X = 60$ pN.

3. Soliton dynamics

For the calculations reported below we used a chain of 25 units at 300 K (unless otherwise mentioned) and a time step of 1.25 fs. The dynamics were followed over 20 ps (16 000 time steps, 2000 CPU s on a Cyber 995E computer). In a typical run ($W = 50$ N m^{-1}; $X = 100$ pN) the norm was conserved to better than 6 ppm and the total energy to better than 0.6 μeV. In figure 2 we show the results of our survey of the (X, W) parameter space at $T = 300$ K.

We recognize immediately that the solitons show up at larger X-values than in case of the averaged Hamiltonian model. However, for small values of W we find that, already for X-values of around 20–40 pN, dispersing solitary waves are formed, followed by regions of dispersive character for increasing X. However, again for $W = 30$ N m^{-1}, in the important region around 50–80 pN, solitons are formed, although they are less stable than in the case of the averaged Hamiltonian method [21].

To discuss some of the cases in more detail we show in figure 3 the time evolution of $|a_n(t)|^2$ for some parameter values. Figure 3(*a*), which shows the case $W = 15$ N m^{-1}, $X = 40$ pN, gives one of the cases where a soliton has already formed for very small values of X, while figure 3(*b*) ($W = 15$ N m^{-1}; $X = 60$ pN) demonstrates that for this larger value of X the soliton has already dispersed rather rapidly into a number of travelling solitary waves. For $W = 30$ N m^{-1} and $X = 50$ pN (figure 3(*c*)) we observe a solitary wave as well as for a larger X-value of $X = 60$ pN (figure 3(*d*)). However, it is obvious that these solitary waves are less stable than in case of the averaged Hamiltonian method [21]. Fully stable travelling solitons, as can be seen from figure 2, show up for much larger values of X than those significant for proteins.

In figure 4 we present the time evolution of $|a_n(t)|^2$ for the parameters $W = 30$ N m^{-1} and $X = 60$ pN for different temperatures. We see immediately that the formation of the solitary wave is a clear temperature effect, since at $T = 0$ K (figure 4(*a*)) the system

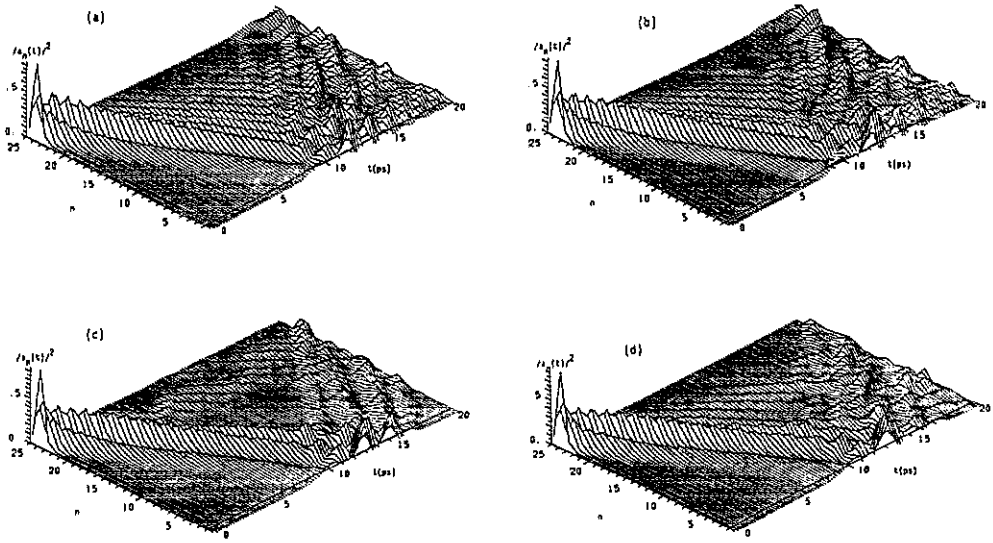

Figure 4. As for figure 3, but for $W = 30$ N m^{-1}, $X = 60$ pN and different values of the temperature: (*a*) $T = 0$ K; (*b*) $T = 100$ K; (*c*) $T = 200$ K; (*d*) $T = 250$ K.

has a dispersive character, while this dispersion is slowed down somewhat at $T = 100$ K (figure 4(*b*)). At $T = 200$ K (figure 4(*c*)) the solitary wave starts to form and at 250 K (figure 4(*d*)) it is clearly visible. Higher temperatures (figure 3(*d*)) again reduce the stability of the solitons. Thus we have to conclude that with increasing temperature in our model the thermal fluctuations first of all effectively decrease the parameter J responsible for dispersion as in the averaged Hamiltonian model, via their implicit influence on the coherent state amplitudes b_{nk} which appear in the real part of the exponents of the coherent state overlaps D_{nm}. However, if the temperature increases further, the fluctuations cause too large a disorder in the system to allow travelling solitons to exist. Thus we have in this case a window of solitary wave formation starting from 200 K. In figure 5 we show for comparison the results obtained with the averaged Hamiltonian model. The case $T = 0$ K is naturally identical with figure 4(*a*). However, in contrast with the thermal phonon distribution discussed above, we see from figure 5(*a*) that at $T = 50$ K the dispersion has already been considerably reduced and at $T = 100$ K (figure 5(*b*)) the solitary wave has started to form. At $T = 150$ K (figure 5(*c*)) we already observe a clear solitary wave which remains qualitatively unchanged up to $T = 300$ K (figure 3(*d*); see also figure 5(*d*) for $T = 250$ K). However, at $T = 350$ K (figure 5(*e*)) the solitary wave has already been destroyed before it is able to reach the chain end. Thus the temperature effects in the averaged Hamiltonian method are qualitatively similar to those in a thermally populated lattice, but far more pronounced. For the averaged Hamiltonian model we observe solitary wave formation from a dispersive system at $T = 0$ K between 150 K and 350 K. The reasons for this behaviour are essentially the same as those described above for the thermally populated lattice vibrations: first the temperature reduces effectively the parameter J via the coherent state overlaps, while a further increase in T leads to too large a disorder owing to thermal lattice fluctuations. The effects here are more pronounced because the temperature appears explicitly in the real part of the exponents of the D_{nm} (see [21] for details), while in the thermally populated phonon case the temperature appears only implicitly via b_{nk} in the real part.

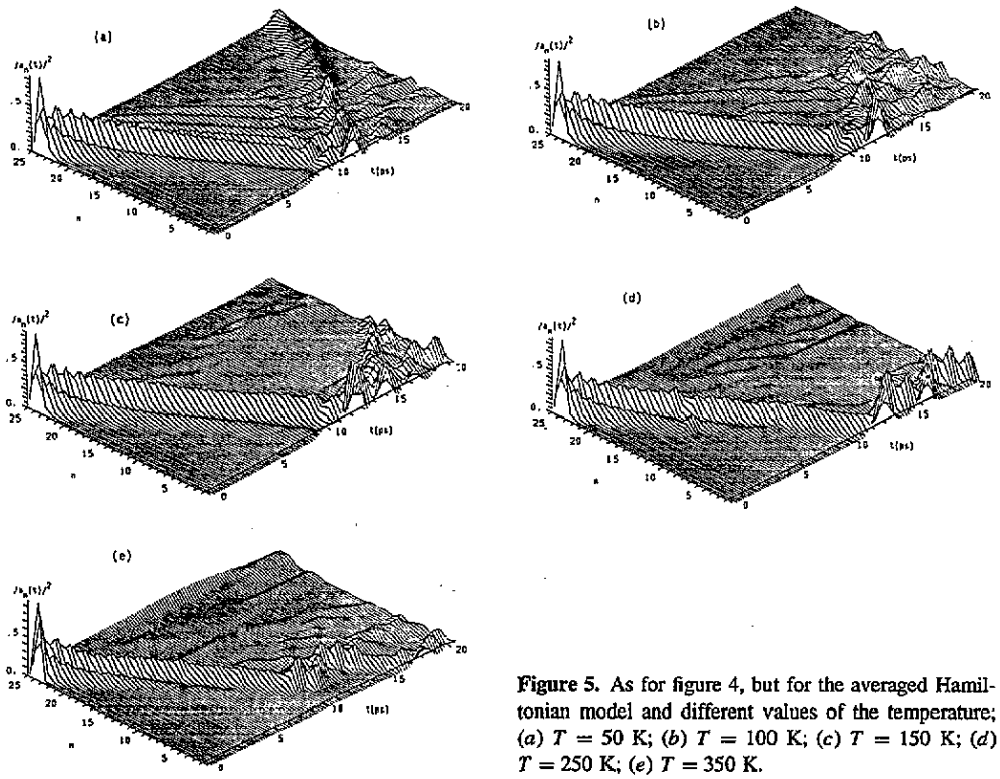

Figure 5. As for figure 4, but for the averaged Hamiltonian model and different values of the temperature; (*a*) $T = 50$ K; (*b*) $T = 100$ K; (*c*) $T = 150$ K; (*d*) $T = 250$ K; (*e*) $T = 350$ K.

Although in both models for temperature effects within the $|D_1\rangle$ *ansatz* state we find solitary waves around the parameter values $W = 30$ N m^{-1} and $X = 60$ pN, there are considerable differences between their stabilities and the sizes of the soliton formation window in the (X, W, T) space. Thus to be able to decide which of the models is more reliable we performed as in [5], for several *ansatz* states, comparisons with exact QMC results published in the literature [21]. This is the topic of the next section.

4. Comparisons with quantum Monte Carlo results from [21]

To be able to do this we introduced periodic boundary conditions and the symmetric interaction into our programs, since this was used in [21]. Details of the procedure have been given in [5]. Thus we restrict ourselves here to a more qualitative description. We concentrate on the parameter values $W = 13$ N m^{-1} and $X = 62$ pN as in [21]. We started the simulation with a random distribution of one vibrational quantum on a ring of 25 units again. Then in each time step we determine the site of maximal amide-I excitation probability and rotate the ring such that this site is the central site (according to the site numbers). Then the quantity $A_n = q_{n+1} - q_{n-1}$ is calculated in this rotated coordinate system and averaged over time. This time average is then compared with the ensemble average of the same quantity obtained by QMC calculations as published in [21]. In [21] peak values of -0.07 Å ($T = 2.8$ K), -0.08 Å ($T = 7.0$ K) and -0.09 Å ($T = 11.2$ K) are reported. This corresponds to coherent structures at 2.8 K, which start to break down at 7.0 K and are completely destroyed at 11.2 K. Thus, only highly localized small polaron-like structures

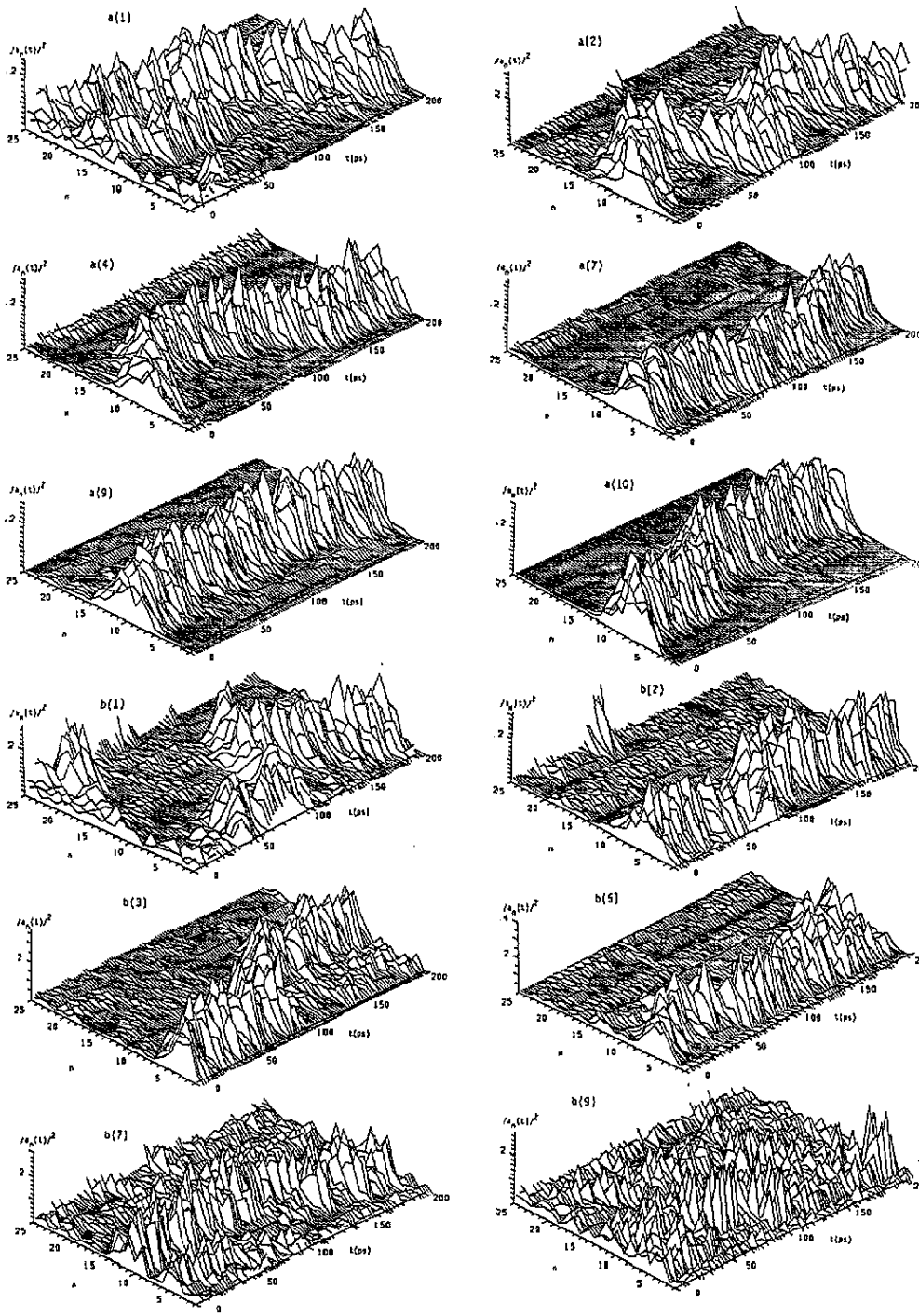

Figure 6. Time evolution of the excitation probability $|a_n(t)|^2$ from an initially randomly distributed amide-I quantum as a function of site n and time t in cyclic chains of 25 units and with symmetric interaction, using the $|D_1\rangle$ *ansatz* state and a lattice with a thermal phonon population prior to the soliton start for different temperatures. The subfigures (numbered 1–10) show six 200 ps parts of the total simulation time of 2 ns. (*a*) $T = 2.8$ K; (*b*) $T = 7.0$ K; (*c*) $T = 11.2$ K.

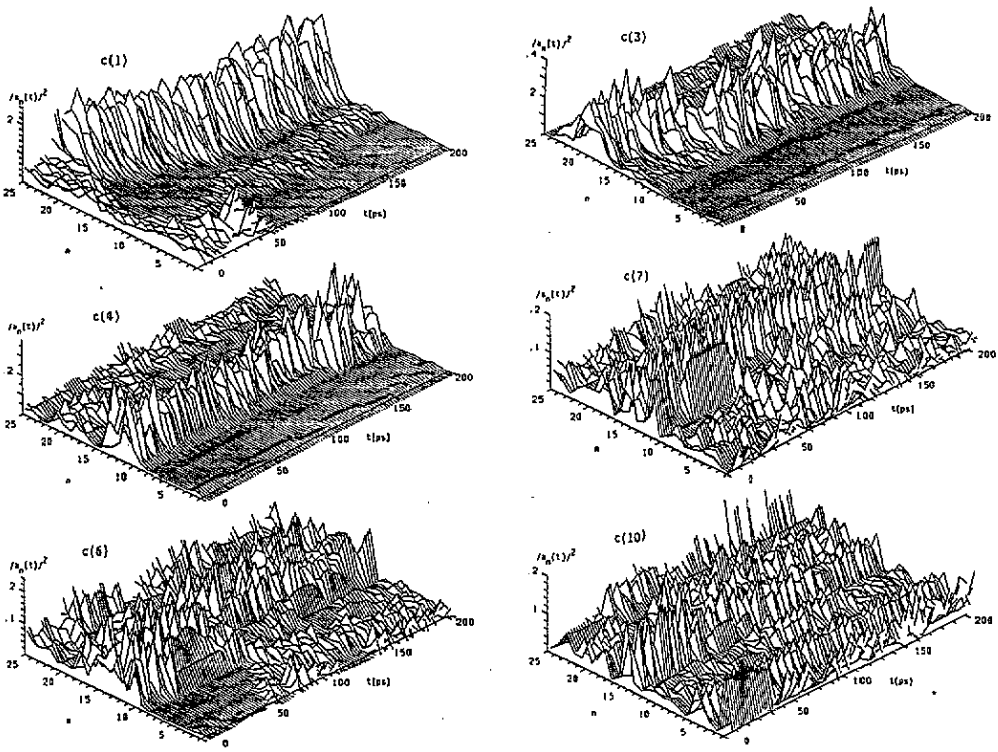

Figure 6. (Continued)

are observed in QMC results. In the case of the averaged Hamiltonian method we have found [5] a qualitatively very similar behaviour. At 2.8 K a travelling soliton is formed from the random initial condition, at 7.0 K the mobility is strongly reduced, while at 11.2 K a highly localized immobile excitation is formed. Although this corresponds qualitatively to the QMC results, the peak values of $\langle A_n \rangle$ were much smaller than the corresponding QMC results and also their variation with temperature is much less pronounced in the averaged Hamiltonian case (we found peak values of -0.026 Å at 2.8 K, -0.028 Å at 7.0 K and -0.029 Å at 11.2 K). These time averages were performed over 3 000 000 time steps, corresponding to 6 ns. After this time the numbers had converged.

For the corresponding calculations with thermally populated lattice vibrations we used a time step of 1 fs and averaged $A_n(t)$ over 2 000 000 time steps, corresponding to a 2 ns simulation time. Each calculation had to be performed with ten restart jobs using 6.7 CPU h each on our Cyber 995E computer. During 2 ns the norm remained conserved to roughly 1 ppb and the total energy to 0.1 neV. In figure 6 we show the time evolution of $|a_n(t)|^2$ for the three temperatures considered, each of them in ten graphs covering 200 ps each. For $T = 2.8$ K (figure 6(a)) from the random initial conditions a solitary wave is formed which becomes trapped after a mobile phase at the beginning of the simulation. However, it is much too broad to be considered as a small polaron-like entity and thus has still to be viewed as a coherent structure as found in the QMC results for this temperature. If the temperature is increased to 7.0 K (figure 6(b)) the localized structure formed is much smaller and less mobile than in the previous case. However, we see that here the localized entity is only an intermediate state and is destroyed after longer times by the thermal fluctuations, leading to a state with a rather random and fluctuating distribution of amide-I excitation. Increasing further the temperature to 11.2 K (figure 6(c)) the intermediate localized state

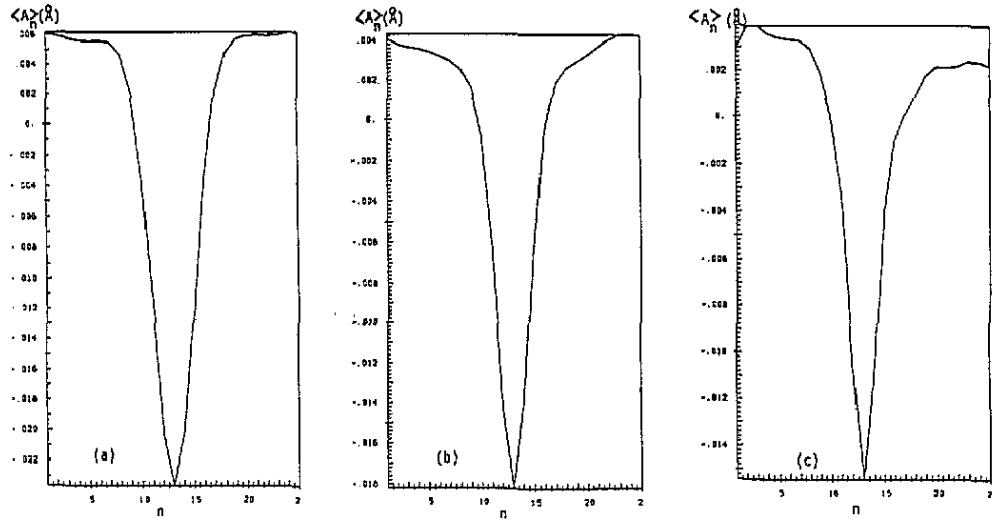

Figure 7. Time average $\langle A_n \rangle$ over 2 000 000 time steps (2 ns) of the lattice displacements A_n in the rotated coordinate system for the system in figure 6 at the same temperatures.

becomes even narrower, but also here is destroyed in the course of the simulation.

In figure 7 we finally show the averaged quantity $\langle A_n \rangle$ for the three temperatures. Also in our case of a thermally populated phonon system the absolute peak values of $\langle A_n \rangle$ are far too small compared with the QMC results and are in absolute values even smaller than the averaged Hamiltonian values. For $T = 2.8$ K we obtain a converged peak value of -0.0235 Å, somewhat smaller in absolute value than the corresponding average Hamiltonian results. However, with increasing temperature the peak value decreases in absolute value (-0.0182 Å at 7.0 K and -0.0154 Å at 11.2 K), while the corresponding QMC and average Hamiltonian results increase. However, for the two higher temperatures, convergence is still not reached, since the excitation is further dispersing. Since the absolute values of the peaks are decreasing, this does not change the conclusion and thus it is not worthwhile to continue the calculations until convergence is finally reached. Therefore, we have to conclude that the average Hamiltonian model has better qualitative agreement with the QMC results than does the thermally populated lattice model and thus has to be preferred.

5. Conclusion

In order to overcome the conceptual difficulties with the average Hamiltonian model for temperature effects in the Davydov theory we have derived equations of motion for the case when the lattice vibrations are thermally populated prior to the soliton start. We found from numerical applications that, in the latter case, solitons are formed at parameter values reasonable for protein helices at 300 K; however, these solitons are less stable than the corresponding solitons in the average Hamiltonian case. A soliton formation window starting from 200 K was found for $W = 30$ N m^{-1} and $X = 60$ pN, while in the average Hamiltonian model the solitons form between 150 K and 350 K. For lower or higher temperatures, respectively, the system is dispersive. Comparisons reveal that the average Hamiltonian model qualitatively agrees with exact QMC results as reported in [5], while the new model does not. Therefore, we conclude that still our previous results from the

averaged Hamiltonian model for one chain [21] as well as for three coupled chains [24] should be qualitatively reliable, apart from the conceptual problems with the *ansatz* of the average Hamiltonian model. These results state that, for parameter values which are realistic for proteins, Davydov solitons should exist at 300 K. However, one should still look for temperature models which also lead to quantitatively more reliable results than the average Hamiltonian model. Work along these lines is in progress in our laboratory.

There are still problems with the quantitative reliability of the $|D_1\rangle$ *ansatz* state even at $T = 0$ K. Thus in a forthcoming paper [26] of this series we shall discuss numerically the errors introduced by the $|D_1\rangle$ *ansatz* in order to obtain some insight into the reliability of results computed with it.

Acknowledgments

The financial support of the Deutsche Forschungsgemeinschaft (project Fo 175/2-3) and the Fonds der Chemischen Industrie is gratefully acknowledged.

References

[1] Davydov A S and Kislukha N I 1973 *Phys. Status Solidi* b **59** 465
Davydov A D 1979 *Phys. Scr.* **20** 387
[2] Davydov A S 1980 *Zh. Eksp. Teor. Fiz.* **78** 789 (Eng. Transl. 1980 *Sov. Phys.–JETP* **51** 397)
[3] Scott A C 1982 *Phys. Rev.* A **26** 57; 1984 *Phys. Scr.* **29** 279
MacNeil L and Scott A C 1984 *Phys. Scr.* **29** 284; 1985 *Phil. Trans. R. Soc.* A **315** 423
[4] Förner W and Ladik J 1991 *Davydov's Soliton Revisited (NATO ASI Series B, vol 243)* ed P L Christiansen and A C Scott (New York: Plenum) p 267
[5] Förner W 1993 *J. Phys.: Condens. Matter* **5** 803
[6] Halding J and Lomdahl P S 1987 *Phys. Lett.* **124A** 37
[7] Lomdahl P S and Kerr W C 1985 *Phys. Rev. Lett.* **55** 1235; 1991 *Davydov's Soliton Revisited (NATO ASI Series B, vol 243)* ed P L Christiansen and A C Scott (New York: Plenum)
Kerr W C and Lomdahl P S 1987 *Phys. Rev.* B **35** 3629
Kerr W C and Lomdahl P S 1991 *Davydov's Soliton Revisited (NATO ASI Series B, vol 243)* ed P L Christiansen and A C Scott (New York: Plenum)
[8] Lawrence A F, McDaniel J C, Chang D B, Pierce B M and Birge R R 1986 *Phys. Rev.* A **33** 1188
[9] Bolterauer H 1986 *Structure Coherence and Chaos, Proc. MIDIT 1986 Workshop* (Manchester: Manchester University Press)
Bolterauer H *Davydov's Soliton Revisited (NATO ASI Series B vol 243)* ed P L Christiansen and A C Scott (New York: Plenum)
[10] Cottingham J P and Schweitzer J W 1989 *Phys. Rev. Lett.* **62** 1792
Schweitzer J W and Cottingham J P *Davydov's Soliton Revisited (NATO ASI Series B, vol 243)* ed P L Christiansen and A C Scott (New York: Plenum)
[11] Motschmann H, Förner W and Ladik J 1989 *J. Phys.: Condens. Matter* **1** 5083
[12] Förner W 1991 *J. Phys.: Condens. Matter* **3** 4333
[13] Förner W 1992 *J. Comput. Chem.* **13** 275
[14] Brown D W, Lindenberg K and West B J 1986 *Phys. Rev.* A **33** 4104, 4110; 1987 *Phys. Rev.* B **35** 6169; 1988 *Phys. Rev.* B **37** 2946
Brown D W 1988 *Phys. Rev.* A **37** 5010
[15] Cruzeiro L, Halding J, Christiansen P L, Skovgaard O and Scott A C 1988 *Phys. Rev.* A **37** 880
[16] Mechtly B and Shaw P B 1988 *Phys. Rev.* B **38** 3075
[17] Skrinjar M J, Kapor D V and Stojanovic S D 1988 *Phys. Rev.* A **38** 6402
[18] Förner W 1991 *Phys. Rev.* A **44** 2694; *J. Mol. Struct.* at press
[19] Förner W 1992 *Nanobiology* **1** 413
[20] Förner W 1992 *J. Phys.: Condens. Matter* **4** 1915
[21] Wang X, Brown D W and Lindenberg K 1989 *Phys. Rev. Lett.* **62** 1796

[22] Scott A C *Conference on Nonlinear Sciences: The Next Decade (Los Alamos National Laboratory, 21 May, 1990)*
[23] Scott A C 1992 *Phys. Rep.* **217** 3
[24] Förner W 1993 *J. Phys : Condens. Matter* **5** 823
[25] Brown D W and Ivic Z 1989 *Phys. Rev.* B **40** 9876
[26] Förner W 1993 *J. Phys.: Condens. Matter* **5** 3897–916